



**HAL**  
open science

## Meaning of xylan acetylation on xylan-cellulose interactions: A quartz crystal microbalance with dissipation (QCM-D) and molecular dynamic study

Zahraa Jaafar, Karim Mazeau, Alexandre Boissière, Sophie Le Gall, Ana Villares, Jacqueline Vigouroux, Nadège Beury, Céline Moreau, Marc Lahaye, Bernard Cathala

### ► To cite this version:

Zahraa Jaafar, Karim Mazeau, Alexandre Boissière, Sophie Le Gall, Ana Villares, et al.. Meaning of xylan acetylation on xylan-cellulose interactions: A quartz crystal microbalance with dissipation (QCM-D) and molecular dynamic study. *Carbohydrate Polymers*, 2019, 226, pp.115315. 10.1016/j.carbpol.2019.115315 . hal-02360093

**HAL Id: hal-02360093**

**<https://hal.science/hal-02360093>**

Submitted on 12 Nov 2020

**HAL** is a multi-disciplinary open access archive for the deposit and dissemination of scientific research documents, whether they are published or not. The documents may come from teaching and research institutions in France or abroad, or from public or private research centers.

L'archive ouverte pluridisciplinaire **HAL**, est destinée au dépôt et à la diffusion de documents scientifiques de niveau recherche, publiés ou non, émanant des établissements d'enseignement et de recherche français ou étrangers, des laboratoires publics ou privés.

1 **Meaning of xylan acetylation on xylan-cellulose**  
2 **interactions: a quartz crystal microbalance with**  
3 **dissipation (QCM-D) and molecular dynamic**  
4 **study**

5 **Zahraa Jaafar<sup>1</sup>, Karim Mazeau<sup>2</sup>, Alexandre Boissière<sup>1</sup>, Sophie Le Gall<sup>1</sup>, Ana Villares<sup>1</sup>,**  
6 **Jacqueline Vigouroux<sup>1</sup>, Nadège Beury<sup>1</sup>, Céline Moreau<sup>1</sup>, Marc Lahaye<sup>1</sup>, Bernard**  
7 **Cathala<sup>1\*</sup>**

8 <sup>1</sup>: INRA, BIA, 44300 Nantes, France

9 <sup>2</sup>: Univ. Grenoble Alpes, CNRS, CERMAV, 38000 Grenoble, France

10

11 \*Corresponding author: [bernard.cathala@inra.fr](mailto:bernard.cathala@inra.fr)

12 \*To whom correspondences should be addressed: [bernard.cathala@inra.fr](mailto:bernard.cathala@inra.fr)

13 Fax: 00 33 (0) 2 40 67 50 68

14 **Other authors' email addresses:**

15 [zahraa.jaafar@inra.fr](mailto:zahraa.jaafar@inra.fr); [karim.mazeau@cermav.cnrs.fr](mailto:karim.mazeau@cermav.cnrs.fr); [alexandre.boissiere@inra.fr](mailto:alexandre.boissiere@inra.fr); [sophie.le-](mailto:sophie.le-gall@inra.fr)  
16 [gall@inra.fr](mailto:gall@inra.fr); [ana.villares@inra.fr](mailto:ana.villares@inra.fr); [jacqueline.vigouroux@inra.fr](mailto:jacqueline.vigouroux@inra.fr); [nadege.beury@inra.fr](mailto:nadege.beury@inra.fr);  
17 [celine.moreau@inra.fr](mailto:celine.moreau@inra.fr); [marc.lahaye@inra.fr](mailto:marc.lahaye@inra.fr);

18

19

20 **ABSTRACT**

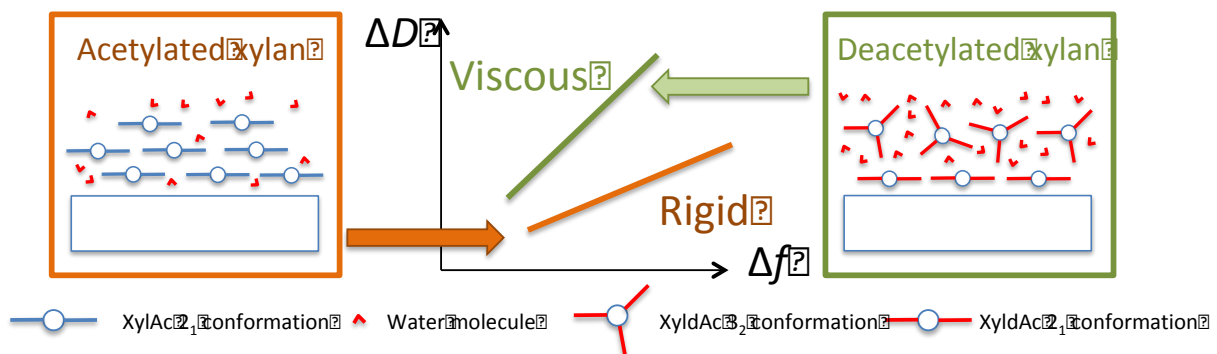
21 In plant cell walls, xylan chains present various substituents including acetate groups. The  
22 influence of the acetyl substitution on the organization of xylan-cellulose complexes remains  
23 poorly understood. This work combines *in vitro* and *in silico* approaches to decipher the  
24 functional role of acetyl groups on the xylan/cellulose interaction. Acetylated xylans were  
25 extracted from apple pomace with dimethyl sulfoxide-lithium chloride (DMSO-LiCl) and  
26 deacetylated using a mild alkali treatment. The adsorption behavior of acetylated and  
27 deacetylated xylan fractions was investigated using quartz crystal microbalance with  
28 dissipation (QCM-D) and molecular dynamics. Acetylated xylans form a dense and poorly  
29 hydrated and rigid layer on cellulose with xylan chains that have two residues per helical turn  
30 conformation, whereas the deacetylated fraction forms a swollen and more viscous layer in  
31 which only the xylan chains in direct contact with the cellulose surface have two residues per  
32 helical turn conformation. The other chains have three residues per turn conformation.

33 **Keywords:**

34 Xylan; acetyl group; cellulose nanocrystal; quartz crystal microbalance with dissipation  
35 (QCM-D); molecular dynamics; hemicellulose.

36

37 **Graphical abstract**



41 **INTRODUCTION**

42 Plant cell walls are highly complex materials that consist of an intricate network of  
43 biopolymers whose main components are polysaccharides. These components include  
44 cellulose, pectin and hemicellulose. As a result of their many uses, their structure and function  
45 *in planta* has been the focus of many studies (Rojas, 2016; Voragen, Schols, & Visser, 2003).  
46 Hemicellulose represents a group of various polysaccharides traditionally extracted by  
47 alkaline treatment from plant cell walls. These polysaccharides in dicots are based on a  $\beta$ -(1-  
48 4) linked backbone of xylose or glucose and/or mannose, forming xyloglucan, xylan, mannan  
49 and glucomannan families (Scheller & Ulvskov, 2010). They exhibit large variations in  
50 composition and structure depending on their botanical origin, tissue type and developmental  
51 stage. This is particularly true of their backbone substitutions with side chains of saccharide  
52 units, hydroxycinnamic acids, methyl ether and acetyl ester groups (Brummell & Schröder,  
53 2009; Gatenholm & Tenkanen, 2004; Scheller & Ulvskov, 2010). Specific substitution  
54 patterns and their role *in planta* remain unclear. Acetyl esterification is a ubiquitous  
55 substitution within hemicellulose families. It usually occurs on O-2 and/or O-3 of xylose in  
56 xylan, on O-6 of galactose and/or mannose, and O-2 and/or O-3 of mannose in  
57 mannan/glucomannan (Melton, Smith, Ibrahim, & Schröder, 2009; Sims, Craik, & Bacic,  
58 1997), and on fucose and/or O-6, O-4 or O-3 of galactose in xyloglucan, although the exact  
59 position has yet to be fully established (Quemener et al., 2015; York, Oates, van Halbeek,  
60 Darvill, & Albersheim, 1988). The alteration of xylan acetyl esterification *in planta* severely  
61 impacts the plant phenotype and its resistance to biotic stresses (Escudero et al., 2017;  
62 Grantham et al., 2017; Kumar, Campbell, & Turner, 2016; Yuan, Teng, Zhong, & Ye, 2016).  
63 From the applied point of view, decreasing xylan acetyl esterification improves enzymatic

64 saccharification in the lignocellulosic biomass biorefinery (Kumar et al., 2016; P. M. Pawar et  
65 al., 2016).

66 Accordingly, understanding the role of the hemicellulose structure in terms of its interactions  
67 with cellulose and its consequences on cell wall architecture and properties remains a key  
68 question in plant development and applications. The present study focuses on the role of  
69 acetyl ester decorations on xylan interactions with cellulose by combining *in vitro* and *in*  
70 *silico* experiments to assess the adsorption features of acetylated and deacetylated xylans.

71 In the case of *in vitro* experiments, a major challenge is the availability of unmodified xylan  
72 fractions since acetyl esters are lost when using classical alkaline hemicellulose extractions.  
73 However, acetylated xylans can be recovered from wood biomass using DMSO extraction,  
74 steam explosion or organosolv pulping (Gatenholm & Tenkanen, 2004). In rich primary cell  
75 wall biomass such as fleshy fruit, acetyl-esterified hemicellulose is recovered after the partial  
76 removal of pectin in the cell wall via dimethyl sulfoxide doped by lithium chloride (DMSO-  
77 LiCl) (Assor, Quemener, Vigouroux, & Lahaye, 2013; Ray, Vigouroux, Quemener, Bonnin,  
78 & Lahaye, 2014).

79 In this study, interactions of acetylated and deacetylated xylan-enriched fractions obtained by  
80 this approach from apple pomace were assessed on a cellulose model surface using quartz  
81 crystal microbalance and dissipation (QCM-D). QCM-D is a highly effective mass-sensing  
82 technique based on the piezoelectric properties of quartz crystals. It has been successfully  
83 used to monitor the hemicellulose adsorption on the cellulose nanocrystal model surface. In  
84 fact, it provides information about the mass adsorbed on the surface as well as the mechanical  
85 behavior of the layer through the measurement of the dissipation factor (Bensselfelt et al.,  
86 2016; Eronen, Osterberg, Heikkinen, Tenkanen, & Laine, 2011; Kohnke, Ostlund, & Brelid,  
87 2011; Villares, Bizot, Moreau, Rolland-Sabate, & Cathala, 2017; Villares, Moreau, Capron, &  
88 Cathala, 2014; Villares, Moreau, Dammak, Capron, & Cathala, 2015). Recently, Villares et

89 al. reported the kinetically-driven xyloglucan adsorption on the cellulose surface and  
90 described a two-regime mechanism (Villares et al., 2015). A similar approach was applied to  
91 investigate the adsorption behavior of acetylated and deacetylated xylan-enriched fractions  
92 referred to as XylAc and XyldAc, respectively, which display different behaviors. As a  
93 complement to the *in vitro* experiment, molecular dynamics (MD) were used to explore the  
94 conformation of xylan chains at the surface of cellulose crystals and to assess their  
95 interactions with water.

96

## 97 **MATERIAL AND METHODS**

### 98 **Chemicals**

99 Dimethyl sulfoxide (DMSO), lithium chloride (LiCl), 37% hydrochloric acid (HCl), orcinol,  
100 standard monosaccharides, sodium tetraborate, 1-methylimidazol, acetic anhydride, sodium  
101 borohydride, ammonia 25%, hydrogen peroxide and dichloromethane were provided by  
102 Sigma-Aldrich Chimie (Saint-Quentin Fallavier, France). Poly(allylamine hydrochloride)  
103 (PAH) was purchased by PolySciences (Mw 120-200 000 g mol<sup>-1</sup>; sodium hydroxide (50%)  
104 (NaOH) by Fluka (Sigma-Aldrich Chimie, Saint-Quentin Fallavier, France); m-  
105 hydroxydiphenyl (MHDP, 3 phenylphenol) by Acros Organics (Geel, Belgium); sulfuric acid  
106 by Fisher Scientific, Illkirch, France; and ethanol 99% by VWR (Fontenay-sous-Bois,  
107 France).

108

### 109 *Cellulose Nanocrystal (CNC) Suspension*

110 Cellulose nanocrystals (CNCs) were obtained by sulfuric acid hydrolysis of cotton linters  
111 according to Revol et al. (Revol, Bradford, Giasson, Marchessault, & Gray, 1992). Cotton  
112 linters were hydrolyzed with 65% wt H<sub>2</sub>SO<sub>4</sub> at 65°C for 35 min (12 g cotton linters/170 mL  
113 H<sub>2</sub>SO<sub>4</sub>). Immediately following hydrolysis, the suspension was diluted 10-fold to stop the

114 reaction and then washed by centrifugation at 10000 rpm for 10 min in order to concentrate  
115 the cellulose and to remove the excess aqueous acid. The resulting precipitate was repeatedly  
116 rinsed **with ultrapure water** and recentrifuged until a colloidal suspension was obtained. The  
117 colloidal suspension was then dialyzed again with distilled water until neutrality (dialysis  
118 membranes MWCO 12-14kDa, Fisher Scientific), after which a mixed-bed research-grade  
119 resin (1 g resin/400 g CNC suspension; Sigma-Aldrich TMD-8) was added to the suspension  
120 for 48 h to remove residual ions. The final aqueous suspension was 2% concentration by  
121 weight (~45% yield). The average crystal dimensions (length and cross-section) measured by  
122 tapping-mode atomic force microscopy (AFM) were 100-200 nm x 6-8 nm. Charges  
123 determined by conductometric titration were equal to 0.098 e/nm<sup>2</sup>.

124

#### 125 *Hemicellulose extraction*

126 Native hemicellulose enriched fractions were sequentially extracted from apple pomace  
127 obtained from the “Institut Français des Produits Cidricoles” (IFPC, Le Rheu, France),  
128 according to the procedure described by Ray et al. (Ray et al., 2014). First, the pectin was  
129 partially extracted from fresh apple pomace (15.6 kg) with 37.5 L of a potassium oxalate  
130 solution (60 mM, pH 4.7, 16 h) at room temperature (~20 °C) and with 3 x 24 L of water (2 x  
131 3 h and 16 h) at 80 °C. After each extraction, the insoluble residue was recovered by manually  
132 pressing through a nylon mesh. The final residue was freeze-dried, weighed and ground  
133 (yield: 79% initial DW). The insoluble residue (200 g) was then incubated with 4 L of  
134 DMSO-LiCl (8.4 wt%; 5 h at 100 °C) under gentle agitation and nitrogen flow. After  
135 centrifugation (11000 g, 15 min, 20 °C), the supernatant was evaporated to dryness using a  
136 rotary evaporator at 70 °C and the dried residue was dissolved in 300 mL of water. Native  
137 hemicellulose was then precipitated with four volumes of ethanol at 4 °C for 16 h. After  
138 centrifugation (11000 g, 15 min, 20 °C), **the dried pellet** was weighed and the yield of

139 DMSO-LiCl extraction was calculated as 5% initial DW. Sixteen g of native hemicellulose  
140 were fractionated by anion exchange chromatography (DEAE- Sepharose Fast Flow column,  
141 5 cm × 15 cm, GE Healthcare, Uppsala, Sweden) (Ray et al., 2014). Elution was performed at  
142 a flow rate of 2 mL min<sup>-1</sup> with water (two column volumes, 600 mL) to recover the unbound  
143 fraction. Bound polysaccharides were eluted using a gradient (six column volumes) from 0 to  
144 1.0 M NaCl. XylAc was recovered in the second carbohydrate eluting peak (~400 mL  
145 elution, ~0.25 M NaCl) determined by colorimetry (see below), dialyzed and freeze-dried  
146 (yield: 500 mg, i.e., 0.14% initial DW). An additional removal of pectin was then performed  
147 by pectin lyase (0.12 U, 3 h at 40 °C, [EC 4.2.2.10] purified from Peclyve Lyven, France)  
148 (Ralet et al., 2012). The XylAc fraction (100 mg) was deacetylated by saponification with 20  
149 mL of 0.5 M NaOH (1 h at 4 °C). After neutralization with HCl, the **deacetylated fraction,**  
150 **referred to as XyldAc,** was desalted by dialysis against deionized water (MWCO 3500 Da,  
151 CelluSep H1) and freeze-dried in order to obtain (the yield is greater than 90% DW of the  
152 XylAc fraction).

153

#### 154 *Hemicellulose characterization*

155 The total neutral sugar content was determined by colorimetry with an automated  
156 orcinol/sulfuric acid assay (Tollier & Robin, 1979). Glucose was used as a standard.

157 Uronic acid content was measured by colorimetry using m-hydroxydiphenyl and concentrated  
158 sulfuric acid hydrolysis (Blumenkrantz & Asboe-Hansen, 1973; Thibault, 1979). The  
159 distinction between galacturonic acid and glucuronic acid was made by comparing  
160 colorimetric responses with and without the addition of sodium tetraborate in the acid,  
161 according to the procedure used by Filisetti-Cozzi, & Carpita (1991). Galacturonic and  
162 glucuronic acids were used as the standard.



163 Identification and quantification of neutral sugars were performed by gas-liquid  
164 chromatography on a TG-225 GC Column (30 x 0.32 mm ID) using a TRACE™ Ultra Gas  
165 Chromatograph (Thermo Scientific™; column temperature: 205 °C; split injector  
166 temperature: 220 °C; flame ionization detector temperature: 250 °C; carrier gas: H<sub>2</sub>) after  
167 sulfuric acid degradation and derivatization as alditol acetates (Dheilly et al., 2016).

168 Acetyl ester content was measured by HPLC as the amount of acetic acid released by  
169 saponification of a 5-mg sample in 1 mL 0.5 M NaOH for 1 h at 4 °C. HPLC was carried out  
170 on a C18 column (4 mm × 250 mm, Lichrospher 100 RP-18e (5 μm), Interchim, France)  
171 thermostated to 25 °C using a refractometric detector (Waters, 2414). An isocratic elution of  
172 4 mM H<sub>2</sub>SO<sub>4</sub> was used at a flow rate of 1.0 mL min<sup>-1</sup> (Levigne, Thomas, Ralet, Quemener, &  
173 Thibault, 2002).

174

#### 175 *Surface preparation*

176 Piezoelectric AT-cut quartz crystals coated with gold electrodes on each side (QSX301, Q-  
177 Sense) were used for QCM-D experiments. Silicon wafers were used for AFM experiments.

178 Quartz crystals and silicon wafers were cleaned with H<sub>2</sub>SO<sub>4</sub>/H<sub>2</sub>O<sub>2</sub> (7:3, v/v), rinsed  
179 exhaustively with Milli-Q water, and dried under a nitrogen stream. Prior to use, QCM-D  
180 quartz sensors were subjected to a plasma-etching device (Harrick Plasma). CNC surfaces on  
181 quartz crystals were prepared by the spin-coating method, as previously described (Villares et  
182 al., 2015). A CNC dispersion at 3 g L<sup>-1</sup> was dropped onto a pre-coated substrate with  
183 poly(allylamine hydrochloride) at 1 g L<sup>-1</sup> in water and accelerated from 180 rpm to 3600 rpm  
184 after 5 min of adsorption and maintained for 60 s at that speed using an expressly designed  
185 spin-coater. The thickness of the CNC layer, evaluated by ellipsometry, was 9 nm ± 5 nm, in  
186 agreement with previous reports (Villares et al., 2017; Villares et al., 2015). Xylan solutions

187 at  $1 \text{ g L}^{-1}$  were then dropped onto wafers pre-coated with CNCs in order to perform AFM  
188 experiments.

189

190 *Quartz crystal microbalance with dissipation (QCM-D) experiments*

191 QCM-D experiments were carried out using a Q-Sense E4 instrument (AB, Sweden). Spin-  
192 coated CNC surfaces were mounted in the QCM-D cells at  $20 \text{ }^\circ\text{C}$  and equilibrated with water  
193 at a flow rate of  $50 \text{ } \mu\text{L min}^{-1}$  until the resonance response was stable. The frequency and  
194 dissipation signals were then offset to zero just before the measurement.

195 Frequency ( $\Delta f_n/n$ ) and dissipation ( $\Delta D_n$ ) changes were simultaneously registered at 5 MHz  
196 fundamental resonance frequency ( $n = 1$ ) and its several overtones as a function of time ( $n =$   
197  $3, 5, 7$ , etc.). The third overtone ( $15 \text{ MHz}$ ,  $n = 3$ ) was used to evaluate the QCM-D data.

198 Xylan solutions at different concentrations ( $0.3$  to  $20 \text{ } \mu\text{g mL}^{-1}$ ) were injected at  $50 \text{ } \mu\text{L min}^{-1}$   
199 and allowed to adsorb for  $40 \text{ min}$  before being exposed again to a water flow in order to  
200 remove loosely-bound material. Each xylan solution at the desired concentration was  
201 adsorbed on a freshly-prepared CNC modified surface and the experiments were repeated at  
202 least three times. All QCM-D experiments were conducted at a constant temperature of  $20 \text{ }^\circ\text{C}$ .  
203 The surface concentration ( $\Gamma$ ) can be calculated from the mass variation during adsorption  
204 obtained from the frequency change ( $\Delta f_n/n$ ) by using the Sauerbrey equation (Sauerbrey,  
205 1959):

206 
$$\Delta m = - C \frac{\Delta f_n}{n}$$

207 where  $C$  is the Sauerbrey constant: constant for the mass sensitivity of the quartz crystal  
208 ( $0.177 \text{ mg m}^{-2} \text{ Hz}^{-1}$  for 5-MHz crystals); and  $n$  is the overtone number. Strictly speaking, the  
209 Sauerbrey equation is valid for ultrathin rigid films whose frequency and dissipation changes  
210 only depend on the mass of the film, especially for adsorbed polymers. A thin film can be  
211 considered to be fully elastic and rigid when  $\Delta D \leq 1 \cdot 10^{-6}$  and no clear spreading of the

212 overtones in the  $\Delta f_n/n$  and  $\Delta D_n$  graphs can be detected. Under such conditions, the Sauerbrey  
213 equation is valid for estimating the mass changes on the sensor surface.

214 A complete description of the kinetic modeling approach is described in Appendix 1 of the  
215 Supplementary Materials (SM).

216

#### 217 *Characterization of CNC surfaces coated with xylan fractions*

218 AFM: Topographical images of silicon wafers were recorded by atomic force microscopy  
219 (AFM) using an Innova AFM (Bruker). The images were collected in tapping mode under  
220 ambient air conditions (temperature and relative humidity) using a monolithic silicon tip  
221 (TESPA, Bruker) with a spring constant of  $42 \text{ N m}^{-1}$  and a nominal frequency of 320 kHz.  
222 Image processing was performed using WSxM 5.0 software.

223

#### 224 *Molecular dynamics (MD) simulations*

225 The models considered in this study consisted of three molecular species: a cellulose  
226 microfibril, xylan chains and water molecules. The cellulose microfibril model contained 18  
227 chains of cellulose (Kubicki et al., 2018) in the I $\beta$  organization and exposed the (110), (1-10)  
228 and (100) surfaces (Mazeau, 2011). The two primitive cell chains of the I $\beta$  allomorph  
229 (Nishiyama, Langan, & Chanzy, 2002) were first duplicated through space, and a P<sub>1</sub> periodic  
230 super-crystal was redefined, which consisted of 6x6 cellulose chains. Each individual chain  
231 consisted of six anhydroglucose units and was covalently bonded to its own periodic image,  
232 mimicking a chain of infinite length. The supercell was then equilibrated using NPT-MD  
233 (constant number of particles, pressure and temperature) at 300 °K and 1 atm. The **a** and **b**  
234 parameters of the periodic cell were then increased to 50 Å and the excess cellulose chains  
235 were removed to retain only 18 chains. The **c** parameter was maintained at its equilibrium  
236 value of 31.4 Å. A charged sulfate group (SO<sub>3</sub><sup>-</sup>) was added on an O-6 oxygen atom of the (1-

237 10) surface to model a cellulose crystal prepared by sulfuric acid, and a Na<sup>+</sup> cation was also  
238 inserted in the simulation box to ensure the neutrality of the system. The model is infinitely  
239 long in the longitudinal direction but finite in the perpendicular direction. This model was  
240 then hydrated using the simple three-point-charges water model (Berendsen, Postma, Van  
241 Gunsteren, & Hermans, 1981) and equilibrated by 50 ns of NVT-MD (constant number of  
242 particles, volume and temperature) at 400 °K. This equilibration resulted in a conformational  
243 change of the hydroxyl and hydroxymethyl groups exposed to the water environment, the  
244 hydroxyl groups created hydrogen bonds with the water molecules, and the surface  
245 hydroxymethyl groups rotated from the *tg* orientation to a mixture of the *gg* and *gt*  
246 orientations. The water molecules were then removed to generate the initial models of the  
247 cellulose-xylan complexes.

248 Xylan chains consisted exclusively of six skeletal anhydroxylose units. They are either non-  
249 substituted or per-acetylated. In the latter case, all of the units were O-acetylated at the O-2  
250 and O-3 oxygen atoms. Two helical conformations,  $2_1$  and  $3_2$ , of the xylan skeleton were  
251 considered. Their coordinates were extracted from a previous study (Mazeau, Moine, Krausz,  
252 & Gloaguen, 2005). For the two helical conformations of the per-acetylated xylan chain, the  
253 initial orientation of the acetyl groups corresponded to the lowest energy extracted from a  
254 Monte-Carlo sampling of 1000 conformations on an isolated chain with a rigid backbone  
255 (SM, Appendix 2).

256 The xylan chains were inserted in the simulation box around the cellulose microfibril. They  
257 were aligned with the microfibril, either parallel or antiparallel at random. Similar to the  
258 cellulose chains, the xylan chains were linked to their periodic images by covalent bonds in  
259 order to mimic infinitely long chains. The two acetylated models, XylAc, consisted of 20  
260 chains of fully acetylated xylan chains (total mass: 25920 g mol<sup>-1</sup>), whereas the two non-  
261 acetylated models, XyldAc, consisted of 33 chains of non-substituted xylan chains (26136 g

262 mol<sup>-1</sup>). Water molecules were then added in the remaining empty spaces of the simulation  
263 boxes.

264 The models were then subjected to energy minimizations followed by MD simulations. The  
265 first energy minimization was performed while maintaining the cellulose and xylan chains  
266 frozen; only the positions of the water molecules were refined at this step. All the atoms were  
267 free to move in the second minimization step. The MD simulations were performed in the  
268 NVT ensemble at 400 °K (50 ns), and then at 298 °K (10 ns). The coordinates of the cellulose  
269 microfibril were frozen during the MDs. MD simulations were long enough to reach  
270 equilibration when the energy, location and conformation of the xylan chains were stable. The  
271 last ns of the room-temperature trajectories were used for analysis.

272

### 273 *Computational details*

274 Material Studio modeling software (v5.5) was used (Accelrys, Inc., San Diego, CA, USA).  
275 Energy calculations were performed using the Universal Force Field (Rappe, Casewit,  
276 Colwell, Goddard, & Skiff, 1992). This all-atoms force field was applied in our previous  
277 study of cellulose-xylan complexes (Mazeau & Charlier, 2012) and it was also used for the  
278 development of a coarse grain force field (Li, Perre, Frank, & Mazeau, 2015). The charge  
279 equilibration method was used to calculate partial charges for each atom (Rappe & Goddard,  
280 1991). The long-range interactions were calculated using the particle-mesh Ewald summation  
281 method (Darden, York, & Pedersen, 1993) with a cut-off distance of 9 Å.  
282 Energy minimization was performed by the steepest descent method and then by the  
283 conjugated gradient method. The convergence criterion was a root-mean-square (rms) force of  
284 less than 0.1 kcal.mol<sup>-1</sup>.Å<sup>-1</sup>. The integration of Newton's laws of motion in the MD  
285 simulations was performed using the standard Verlet algorithm (Verlet, 1967) with a time step

286 of 0.001 ps. The total external pressure was maintained at 1 atm (Berendsen et al., 1981) and  
287 a Hoover algorithm (Evans & Holian, 1985) was used to keep the cell temperature constant.

288

289

## 290 **RESULTS**

### 291 *XylAc and XylAc fractions extraction and characterization*

292 Investigation of the hemicellulose function in the plant cell wall requires careful extraction in  
293 order to provide a structure representative of those naturally occurring *in planta*. However,  
294 hemicellulose is classically extracted with alkali, leading to the hydrolysis of the acetyl ester  
295 groups. In a previous study, a non-aqueous polar aprotic solvent, namely DMSO doped with  
296 LiCl, was used to efficiently extract acetyl-esterified hemicelluloses (Assor et al., 2013; Ray  
297 et al., 2014). Applying this extraction procedure to apple pomace after partial removal of  
298 pectin followed by anion exchange chromatography allowed the recovery of a xylan-enriched  
299 fraction (XylAc). Fig. S1 reviews the overall extraction process. The extract was composed in  
300 decreasing order of weight proportion as follows: xylose, uronic acid, arabinose and acetyl  
301 esters, as well as low amounts of glucose, galactose and mannose and traces of fucose (Table  
302 1). Mild alkali treatment of the fraction succeeded in removing acetyl esters with limited  
303 changes in the sugar composition (Table 1). **The extract was thus mainly enriched in**  
304 **arabinoxylan (GAX), whose composition was close to that reported for Gala GAX (Ray et al.,**  
305 **2014) except for the presence of glucuronic acid, though comparatively richer in acetyl esters**  
306 **(7.2% vs. 3.8% in Gala). The presence of low amounts of glucose, mannose, galactose and**  
307 **fucose indicates the likely contamination of the AX by some galactoglucomannan and**  
308 **xyloglucan, whereas the galacturonic acid and rhamnose content suggests the presence of**  
309 **remaining pectin.** Assuming that all acetyl esters were related to the xylan and were linked to  
310 the xylose residue, there would be one acetyl group for approximately two xylose residues, in

311 agreement with the average distribution of acetyl ester in plant xylan (Busse-Wicher et al.,  
 312 2014; Chong et al., 2014; Grantham et al., 2017). Glucuronic acid and arabinose are present in  
 313 the proportion of one uronic acid for approximately three xyloses, instead of one to six  
 314 xyloses in the *Arabidopsis* primary wall and one arabinose for approximately 3.4 xylose  
 315 residues, which could account in part for the pentose unit linked to glucuronic acid in the  
 316 *Arabidopsis* primary wall xylan (Mortimer et al., 2015).

317

318 Table 1. Chemical composition of the acetylated (XylAc) and deacetylated (XyldAc) xylan  
 319 fractions. Total sugars (TS) and the acetyl group contents are expressed in wt% and  
 320 monosaccharide content is expressed in mol%.

	<i>Acetyl</i>	<i>TS</i>	<i>Glc</i>	<i>Gal</i>	<i>Man</i>	<i>Xyl</i>	<i>Ara</i>	<i>Fuc</i>	<i>Rha</i>	<i>GalA</i>	<i>GlcA</i>
	(wt%)		(mol%)								
XylAc	7.2	78.3	5.4	5.1	2.3	51.9	16.5	0.2	1.0	16.5	1.0
XyldAc	0	77.6	4.9	5.0	2.7	53.6	16.9	0.3	1.0	14.8	0.9

321

### 322 *Adsorption of XylAc and XyldAc fractions on the cellulose model surface*

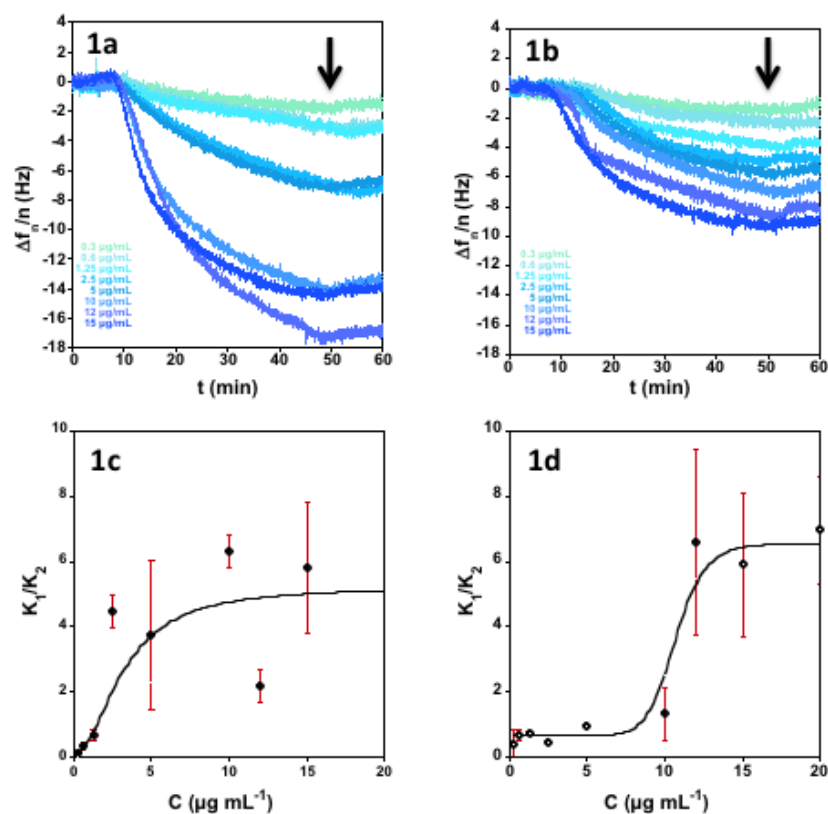
323 Spin-coated CNCs prepared from cotton linters were used as a model surface. They displayed  
 324 the expected rod-like morphology with dimensions of approximately 175 nm in length, 15 nm  
 325 in width and 7 nm in thickness, consistent with previous reports (Cherhal, Cousin, & Capron,  
 326 2015). The ability of XylAc and XyldAc-enriched fractions to adsorb on the CNC surface was  
 327 evaluated and compared by QCM-D. This technique relies on the properties of piezoelectric  
 328 quartz sensors submitted to an electric field that induces mechanical shear wave of the crystal.  
 329 Adsorption of any material on the quartz surface induces a shift in the frequency resonance  
 330 ( $\Delta f_n$ ), allowing real-time monitoring of polymer adsorption on the quartz surface. Thanks to  
 331 its very high sensitivity, the technique has been successfully used to monitor a wide range of

332 adsorption processes. The second piece of information that can be obtained from the QCM-D  
333 analysis is the dissipation factor  $\Delta D$ . This value provides an indication of the mechanical  
334 (viscoelastic) behavior of the layer adsorbed on the quartz since it reflects how the layer will  
335 dissipate the energy of the oscillation waves of the quartz sensor. QCM-D has already been  
336 used for the investigation of adsorption of xylan and xylan derivatives (Dammak et al., 2013;  
337 Kohnke et al., 2011; Sang Hoon Lee, Lee, & Youn, 2014; S. H. Lee, Lee, & Youn, 2015).  
338 Prior to QCM-D analysis, the xylan fractions were adsorbed on the CNC surfaces and the  
339 morphology was analyzed by atomic force microscopy (Fig. S2). In all the cases, the CNCs  
340 were easily visible and the complexes showed no clear differences with the initial CNC  
341 surface. This indicates that xylan is adsorbed as an individual polymer chain or, at most, as  
342 very small aggregates undetectable by AFM. In the following section, we report the frequency  
343 variations for different hemicellulose fractions, followed by an investigation of the dissipation  
344 patterns.

345 *Frequency variation during XylAc and XyldAc adsorption and kinetic modeling of the*  
346 *adsorption behaviors*

347 Prior to injection, the CNC surfaces were stabilized with water and the xylan fractions were  
348 injected at different concentrations ranging from  $0.3 \mu\text{g mL}^{-1}$  up to  $20 \mu\text{g mL}^{-1}$  to explore a  
349 large panel of ratios between polymers and adsorption sites. For the two fractions, acetylated  
350 and deacetylated, the decrease of frequencies observed, regardless of the concentration  
351 injected, indicated adsorption of xylan fractions on the cellulose surface. For each xylan  
352 concentration, adsorption was repeated at least three times to assess the reproducibility, and a  
353 typical frequency variation against time is reported in Fig. 1. Adsorption was irreversible  
354 since the rinsing steps applied after adsorption (indicated by arrows on Fig. 1) did not change  
355 the frequency values.





356

357 **Fig. 1.** Frequency ( $\Delta f_n$ ) (3<sup>rd</sup> overtone) for the adsorption of XylAc (1a) and XyldAc (1b)  
 358 fractions and evolution of the  $k_1/k_2$  ratio as a function of the XylAc (1c) or XyldAc (1d)  
 359 concentration (solid lines are visual guides). Arrows indicate the beginning of the rinsing step  
 360 with water.

361

362 For the XylAc and XyldAc fractions, different maximal frequency values were obtained for  
 363 all concentrations studied, indicating that the final amount of xylan adsorbed depended on the  
 364 sample concentration applied, as previously reported for the xyloglucan adsorption on CNC  
 365 surfaces (Villares et al., 2017; Villares et al., 2015). Frequency variations were in the same  
 366 range (tens of Hz) for both xylan fractions, suggesting that the amounts adsorbed are similar,  
 367 contrary to Kabel *et al* results that reported a higher adsorption of the deacetylated fraction.  
 368 (Kabel, van den Borne, Vincken, Voragen, & Schols, 2007). This finding can be assigned to

369 a lower steric hindrance due to the removal of acetyl groups to increase the self-associative  
370 capacity of xylans, as reported earlier by Linder (Bosmans et al., 2014; Linder, Bergman,  
371 Bodin, & Gatenholm, 2003). Since both the XylAc and XyldAc fractions did not desorb from  
372 the surface during the time scale of the experiment, the maximal frequencies cannot be  
373 attributed to a dynamic equilibrium between adsorption and desorption of the polymer.  
374 Moreover, the continuous flow of XylAc and XyldAc on the surface guaranteed that the  
375 maximum coverage possible for each condition was reached. Thus, this pattern suggests that  
376 the final amount of polymer adsorbed depended on the competition between adsorption,  
377 packing optimization and potential rearrangement, suggesting that the adsorption process is  
378 therefore not the result of thermodynamic equilibrium but, instead, is kinetically-driven.

379 We previously described such behavior by using a kinetic model that comprises two steps: the  
380 first one describes the adsorption of hemicellulose onto an uncovered surface associated with  
381 the rearrangement of the chains to cover the surface, and the second corresponds to adsorption  
382 on a covered surface on which the polymer must diffuse through a pre-adsorbed  
383 hemicellulose layer (Villares et al., 2017). This kinetic model was used to determine  $k_1$  and  $k_2$   
384 for the XylAc and XyldAc fractions that are the kinetic constant for the first and second  
385 adsorption steps, respectively. The detailed mathematical expressions of the kinetic model  
386 and typical fits obtained are given in the Supplementary Material (SM, Appendix 1). The  
387 experimental fractional coverage was calculated to obtain values of the kinetic constants  $k_1$   
388 and  $k_2$ , and there was a good fit between experimental and calculated values (Fig. S3). The  
389 evolution of the ratio  $k_1/k_2$  against the XylAc and XyldAc fraction concentration is plotted in  
390 Fig. 1c and d, respectively. The fractions display different patterns with two domains of  
391 concentrations.

392 At low concentration, the  $k_1/k_2$  ratio is lower or close to one indicating that the kinetic  
393 adsorption and lateral rearrangement occur at a similar time scale, leading to large amounts of

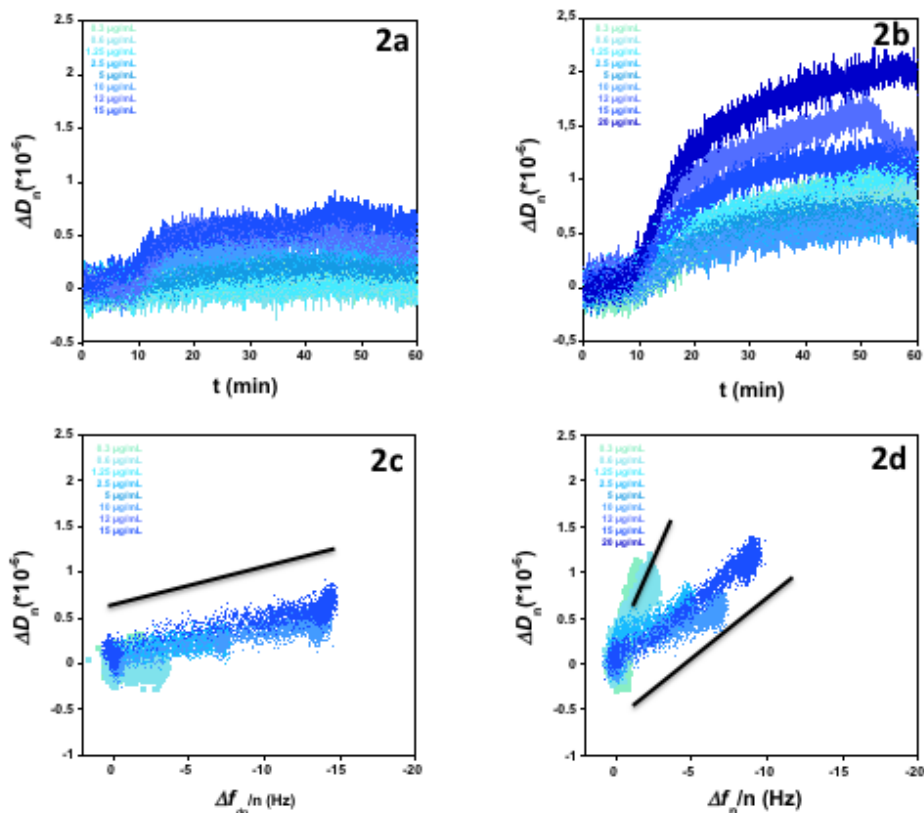
394 extended xylan conformation or trains. At higher concentrations, adsorption occurs through  
395 diffusion on the pre-adsorbed layer, and the crowding of the surface limits diffusion and  
396 rearrangement mechanisms. Thus, the  $k_1/k_2$  ratio increases since the adsorption process on a  
397 bare surface ( $k_1$ ) dominates, while ( $k_2$ ) decreases dramatically. The increase of the  $k_1/k_2$  ratio  
398 associated with a higher amount of polymer adsorbed can be interpreted either by a denser  
399 packing of the molecules when the concentration increases or by limited rearrangement  
400 possibilities. A clear difference can be seen between acetylated and deacetylated xylan. In the  
401 case of the XylAc fraction, the  $k_1/k_2$  ratio increases very rapidly, suggesting that even at low  
402 concentrations, the acetylated sample is able to efficiently cover the surface and the  
403 possibility of rearrangement seems to be strongly limited, suggesting efficient interactions  
404 between XylAc and the cellulose surface. In the case of XyldAc, a transition between the two  
405 regimes (i.e., the concentration at which the  $k_1/k_2$  ratio increases) is clearly seen at around 5-  
406  $10 \mu\text{g mL}^{-1}$ . This suggests that chain rearrangements can occur at low surface concentrations,  
407 whereas surface crowding may limit conformation modification at higher concentrations.  
408 Nevertheless, the presence of acetyl groups changes the adsorption behavior of the xylan  
409 chains and the acetylated fraction seems to have a greater ability to cover the surface than the  
410 deacetylated one.

#### 411 *Comparison of the viscoelasticity behaviors of adsorbed layers*

412 To correlate the evolution in dissipation with changes in frequency, the  $\Delta D$  was plotted as a  
413 function of  $\Delta f$  (hereafter referred to as  $\Delta D$  vs.  $\Delta f$  plots) to eliminate time as an explicit  
414 parameter (Fig. 2). The raw dissipation data for both fractions at different concentrations are  
415 illustrated in Figs. 2a and 2b. The  $\Delta D$  vs.  $\Delta f$  plots revealed different slopes of the curves that  
416 are related to the overall viscoelasticity of the layer. A rigid layer will behave similarly to the  
417 quartz dissipation and the  $\Delta D$  will present low values per mass addition and, accordingly, the  
418  $\Delta D$  vs.  $\Delta f$  slope will be low. In the case of a more viscoelastic layer, the  $\Delta D$  vs.  $\Delta f$  slope will

419 display higher values. As shown in Figs. 2c and 2d, the two xylan fractions display strikingly  
420 different behaviors. The slope obtained for XylAc is constant ( $0.03 \cdot 10^{-6} \text{ Hz}^{-1}$ ) regardless of the  
421 concentration studied, indicating that irrespective of concentration, the adsorbed acetylated  
422 xylan layer on cellulose shares a similar organization. Moreover, the very low value of the  
423 slope suggests that the adsorbed layer is rigid. This finding is consistent with the kinetic  
424 analysis that displays only one regime of adsorption in which the  $k_f$  constant is dominant and  
425 which suggests that the XylAc layer is strongly adsorbed with limited diffusion and  
426 rearrangement processes. It should be emphasized that the slope value of the  $\Delta D$  vs.  $\Delta f$  of  
427 XylAc is significantly lower compared to the values found in the literature. For example,  
428 Eeronen et al. (Eeronen et al., 2011) reported a value of  $0.25 \cdot 10^{-6} \text{ Hz}^{-1}$  for wheat arabinoxylans  
429 and of  $0.1 \cdot 10^{-6} \text{ Hz}^{-1}$  for spruce galactoglucomanans, which are on the same order of magnitude  
430 as the value measured for the XyldAc but almost ten times higher than the value of  $0.03 \cdot 10^{-6}$   
431  $\text{ Hz}^{-1}$  determined for the XylAc. This finding suggests that the mechanical properties of the  
432 XylAc layer are quite similar to those of the cellulose surface and can probably be attributed  
433 to flat and dense layers.

434 In contrast, the  $\Delta D$  vs.  $\Delta f$  plot of XyldAc displays different slopes depending on the injection  
435 concentration, indicating a more complex behavior (Fig. 2d). The  $\Delta D$  vs.  $\Delta f$  plot pattern  
436 evolved during the adsorption process, suggesting a change in layer organization during  
437 adsorption. At low concentrations ( $<5 \mu\text{g mL}^{-1}$ ), the slope value is around  $0.25\text{-}0.5 \cdot 10^{-6} \text{ Hz}^{-1}$ ,  
438 whereas at higher concentrations, the value decreases to  $0.1\text{-}0.15 \cdot 10^{-6} \text{ Hz}^{-1}$ . At low  
439 concentrations, the slope value is high, which indicates a high viscosity of the layer, and then  
440 starts to decrease to reach a stable value at a concentration of  $5\text{-}10 \mu\text{g mL}^{-1}$ . This suggests the  
441 formation of a loose layer that becomes denser as the concentration increases.



442

443 **Fig. 2.** Dissipation ( $\Delta D$ ) ( $3^{\text{rd}}$  overtone) for the adsorption of XylAc (2a) and XyldAc (2b)  
 444 fractions for different concentrations as a function of time and corresponding  $\Delta D$  vs.  $\Delta f$  plots  
 445 for XylAc (2c) and XyldAc (2d) (solid lines are visual guides).

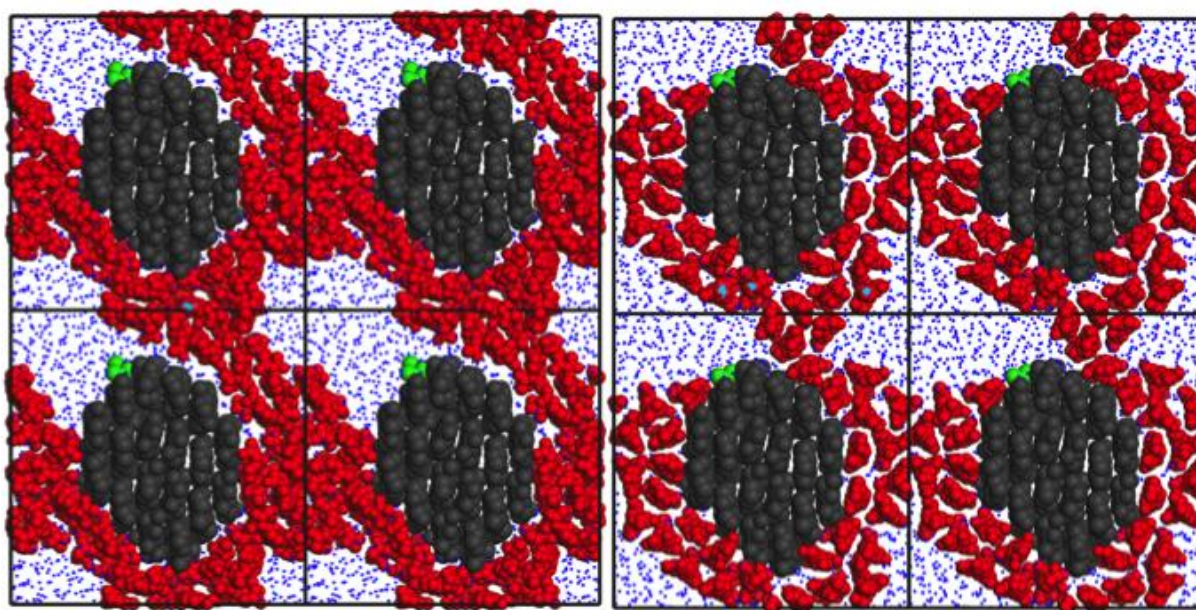
446

447 *Adsorption of XylAc and XyldAc fractions on the cellulose model surface by MD*

448 Four models of the hydrated cellulose xylan complex that differed by the chemical structure  
 449 of their xylan chains and by their initial conformation were considered. The xylan chains were  
 450 either acetylated or non-acetylated (corresponding to deacetylated sample). Repeat unit is  
 451 shown in Fig S4. In addition, to account for the conformational polymorphism of xylan  
 452 (Chanzy, Dube, & Marchessault, 1979; Larsson, 2004; Teleman, Larsson, & Iversen, 2001),  
 453 the xylans differed by the initial helical conformation of their backbone: either two units per  
 454 helical turn when the xylan chains contained three turns of the  $2_1$  helix in their initial state, or

455 three units per helical turn when they contained two turns of the left-handed  $3_2$  helix (Figs. S5  
456 and S6).

457 The four models were subjected to MD simulations at two temperatures. During the high  
458 temperature phase, the xylan chains explored the two helical conformations with rapid inter-  
459 conversions between the two forms. This is not surprising since the two conformations have  
460 similar energies and the energy barrier between them, estimated from the adiabatic potential  
461 energy surface of xylobiose (Mazeau, Moine, Krausz, & Gloaguen, 2005), is lower than 2  
462 kcal mol<sup>-1</sup>. In contrast, during the room-temperature phase, each xylan chain stabilized in its  
463 preferred conformation depending on its immediate environment and remained in that  
464 conformation up to the end of the trajectory. As a consequence, the models that differed by  
465 the initial conformation of the xylan chains converged into an identical structure of the  
466 complex. Fig. 3 provides representative snapshots of the XylAc and XyldAc models.



467  
468 Fig. 3: Cross-sectional views of the models of the hydrated cellulose-xylan complexes. 2x2  
469 basic cells are displayed. Hydrogen atoms are omitted for clarity. Cellulose is in gray. Sulfate  
470 group, in green, is located on a chain of the (1-10) surface of cellulose next to its top corner.

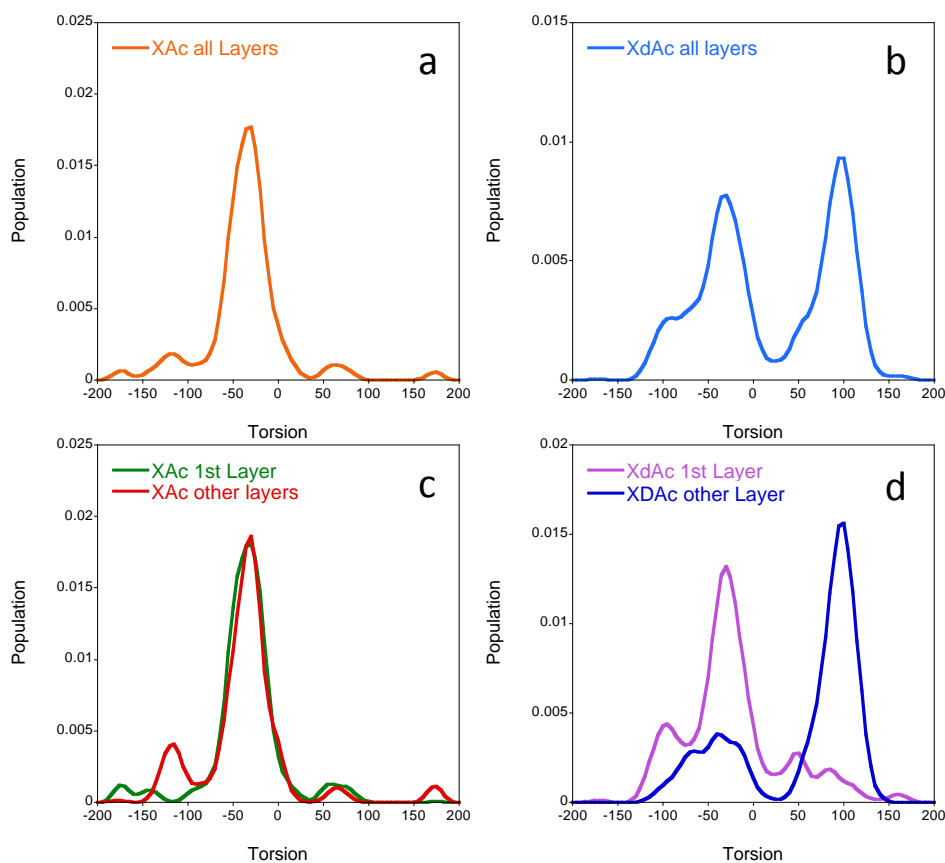
471 The xylan chains are in red and the water molecules in blue. Left: XylAc model; right XyldAc  
472 model.

473

#### 474 *Conformation of the xylan chains*

475 Analysis of the helical conformations of the xylan chains in the equilibrated models is  
476 performed using the turn angle (T), which is defined by the sequence of atoms O-5''-C-  
477 5''-C-4-C-5 (Fig. S4). The turn angle describes the orientation of a given unit with respect to  
478 its second neighbor for those perfectly stereo-regular helices that were used to build the initial  
479 models  $T = -50^\circ$  for the  $2_1$  helix and  $T=100^\circ$  for the  $3_2$  helix.

480 Fig. 4 gives the distributions of the turn angle of the xylan chains in the equilibrated XylAc  
481 and XyldAc models. It shows the distributions of all the chains (denoted 'all'), together with  
482 that of the chains in close proximity to the cellulose, denoted '1<sup>st</sup> layer', and that of the chains  
483 far from the cellulose, denoted 'other layer'. For the purpose of comparison, the same  
484 calculations were performed for arged cellulose, and similar distributions were obtained in all  
485 cases (SM, Appendix 3 - Fig. S10 - S11-S12).



486

487 **Fig. 4.** Distribution of the turn angle in the XylAc (left) and XyldAc (right) simulated  
 488 systems Global distributions from all the xylan chains (4a and 4b); and distributions from the  
 489 xylan chains interacting with cellulose (orange in 4c and light blue in 4d) and from the bulk  
 490 xylan (red in 4c and dark blue in 4d).

491

492 For XylAc, the distribution is almost monomodal and centered at  $T = -35^\circ$ . Considering the  
 493 thermal motion and local conformational variability, this peak corresponds to helices with two  
 494 residues per helical turn. The distribution of  $T$  also reveals other forms, non-canonical, less  
 495 organized and of low occurrence, at  $T = -120^\circ$ ,  $60^\circ$  and  $180^\circ$ . Conformations of the xylan  
 496 chains in the XyldAc model differ substantially. The bimodal distribution of the turn angle  
 497 centered at  $T = -35^\circ$  and  $+95^\circ$  shows that the deacetylated xylan chains explore the two main  $2_1$   
 498 and  $3_2$  helical forms. It should be noted that most of the chains in direct interaction with



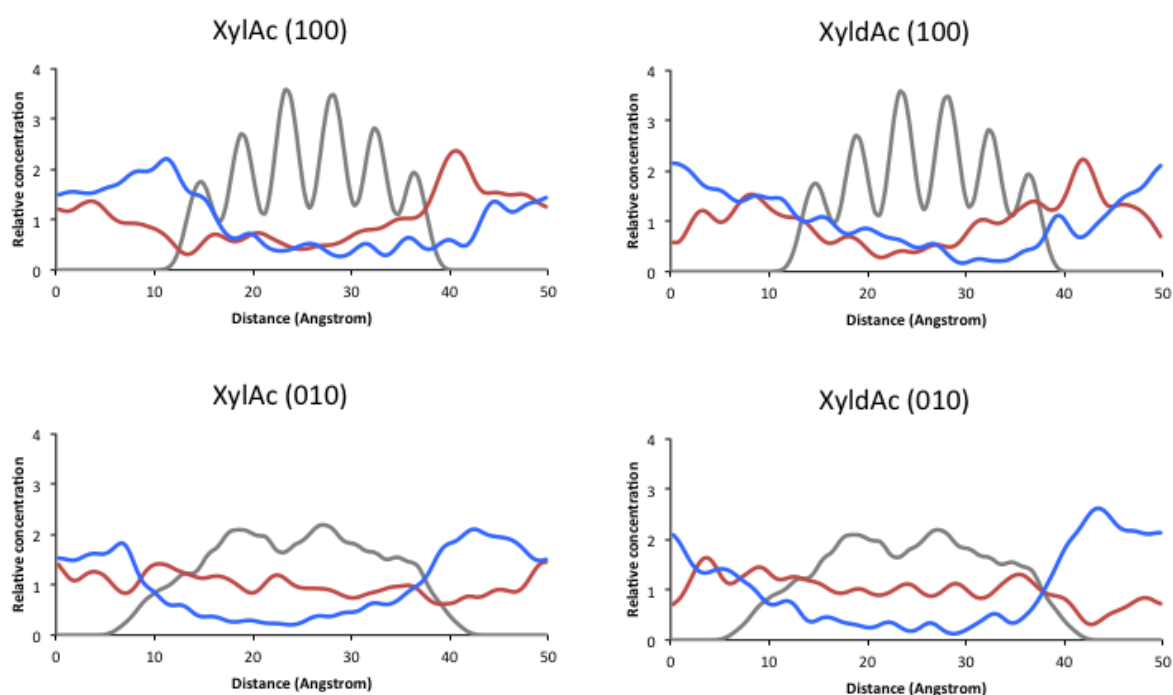
499 cellulose are mainly in the  $2_1$  conformation, whereas those far from the cellulose (in the bulk  
500 phase of xylan) are in the  $3_2$  conformation. Here again, a few chains explored alternative  
501 disorganized conformations, as suggested by the broad distribution of the turn angle.

#### 502 *Concentration profiles.*

503 The concentration fluctuations of cellulose, xylan and water were determined along the 100  
504 and 010 directions in both the immediate environment of the cellulose and in the bulk xylan  
505 (Fig. 5).

506 At the interface with cellulose, the acetyl groups do not affect the adsorption behavior of  
507 xylan. The concentration traces at 40 Å show a maximum for xylan and, concomitantly, a  
508 minimum for water, which is particularly visible on the profiles along the 100 direction. This  
509 reveals that xylan accumulates at the interface on the uncharged side of the cellulose crystal.  
510 The concentration profiles of xylan and water at the interface with cellulose are, however,  
511 dissymmetrical. At 10 Å in the plots, i.e., on the charged side of the cellulose, the xylan  
512 concentration is minimal, whereas that of water is maximal, which suggests that the charged  
513 sulfate group preferentially interacts with the surrounding water molecules rather than with  
514 xylans. Additional modeling was performed with a native (uncharged) cellulose crystal in  
515 order to estimate the exact effect of the charged sulfate group (see SM, Appendix 3, Figs. S11  
516 and 12). The corresponding concentration traces with uncharged cellulose are in fact more  
517 symmetrical and show a high concentration of xylan and a low concentration of water at both  
518 interfaces. The charged sulfate group does not interact with the acetylated xylans but can  
519 occasionally form a hydrogen bond with a hydroxyl group of the deacetylated xylan. The  
520 charged sulfate group, along with its surrounding hydration shell, enhances the cellulose  
521 hydrophilicity, increases the porosity of the total system, and lowers the total cellulose surface  
522 covered by xylan.

523 In contrast, within the xylan phase, at around 0 or 50 Å in the concentration profiles, the  
 524 acetyl groups have a strong influence on xylan organization. For XylAc, xylan concentration  
 525 is similar to that of water, suggesting that the system is dense and weakly hydrated. This type  
 526 of organization is obviously facilitated by the dominant  $2_1$  helical conformation of their  
 527 backbones whose compact packing, similar to that of cellulose or chitosan, can be easily  
 528 achieved. However, the multiple conformations explored by the acetyl groups disturb the  
 529 perfection of the packing at the local level and create small cavities in which few water  
 530 molecules can penetrate. For XyldAc, in contrast, xylan concentration is much lower than that  
 531 of water, which suggests that the deacetylated xylan layer is loose and highly hydrated. The  
 532 two free hydroxyl groups per repeat unit strongly interact with water molecules and the  
 533 packing of the  $3_2$  helices promotes uninterrupted columns of water that appear in between the  
 534 deacetylated xylan chains.



535  
 536 Fig. 5: Concentration profiles of cellulose, xylan and water along directions perpendicular to  
 537 the exposed crystallographic planes of the cellulose. In gray: cellulose; in red: xylan; in blue:  
 538 water.

539 Our models are consistent with experimental data from X-ray diffraction and solid-state  
540 NMR. The crystal structure of xylan diacetate is anhydrous and made of two-fold helices  
541 (Gabbay, Sundararajan, & Marchessault, 1972), whereas that of deacetylated xylan contains  
542 between one to three water molecules per xylosyl unit and the chains are in the left-handed  
543 three-fold helix (Nieduszynski & Marchessault, 1971; Nieduszynski & Marchessault, 1972).  
544 These deacetylated xylan chains also explore the three-fold conformation in a water solution  
545 but change their conformation to the two-fold one when interacting with cellulose (Larsson,  
546 Hult, Wickholm, Pettersson, & Iversen, 1999). It should be noted that such conformational  
547 adaptation is limited to those xylan chains in direct contact with the cellulose surface (Falcoz-  
548 Vigne et al., 2017).

549 In a modeling study, the two limiting cases were studied where xylan chains are either per-  
550 acetylated or deacetylated, whereas Busse-Wicher et al. modeled the adsorption of a partly-  
551 acetylated xylan chain in which the distribution of the acetyl groups is stereoregular, i.e.,  
552 where every other xylose residue is acetylated (Busse-Wicher et al., 2014). Comparing the  
553 two studies makes it possible to determine the effects of the degree of acetylation in the xylan  
554 chain on its interaction with cellulose. The degree of acetylation does not affect the  
555 conformation of xylan in direct contact with cellulose, adopting the two residues per helical  
556 turn conformation. Acetylation also does not affect the adsorption features of xylan on the  
557 hydrophobic surface of cellulose. Instead, it stacks on this surface by its aliphatic C-H groups.  
558 The interaction on this particular cellulose surface is dominated by the Van der Waals forces  
559 (Martinez-Abad et al, 2017; Mazeau & Charlier, 2012). In contrast, the degree of acetylation  
560 affects the adsorption features of xylan on the hydrophilic surfaces of cellulose. The per-  
561 acetylated xylan adsorbs flat to maximize the number of Van der Waals contacts. This  
562 organization is obviously promoted by the amphiphilicity of the cellulose surfaces (Mazeau,  
563 2011). On the contrary, the deacetylated xylan adsorbs in a tilted conformation to establish

564 hydrogen bonds between its hydroxyl groups and the hydroxyl groups protruding from the  
565 cellulose surface. The regularly and alternately substituted xylan considered by Busse-Wicher  
566 et al., which forms hydrogen bonds with cellulose, thus follows the adsorption of the non-  
567 substituted xylan (Busse-Wicher et al., 2014). This similarity is understandable considering  
568 that a xylan polymer in the  $2_1$  helical conformation in which only one residue out of two is  
569 substituted has only one acetylated side. This is the non-substituted side, consisting only of  
570 hydroxyl groups, that preferentially interacts with cellulose in the same way as a deacetylated  
571 xylan.

572

## 573 **DISCUSSION**

574 Xylan presents a broad structural variability and is a major hemicellulose in plant biomass,  
575 essentially encountered in secondary cell walls (Brummell & Schröder, 2009; Scheller &  
576 Ulvskov, 2010). It is, however, a minor component of primary cell walls and particularly  
577 those of fleshy fruit (Brummell & Schröder, 2009) such as apple where it occurs as  
578 glucuronoarabinoxylan (GAX) (Ray et al., 2014). The proportions of uronic acids, arabinose  
579 and acetyl ester substitutions determined for the apple pomace xylan fractions are similar to  
580 those reported for Gala apple (Ray et al., 2014). Considering that apple pomace is not  
581 lignified, it is therefore a convenient biological source for native xylan with a preserved  
582 substitution pattern that can be used as a model polymer for *in vitro* investigation.

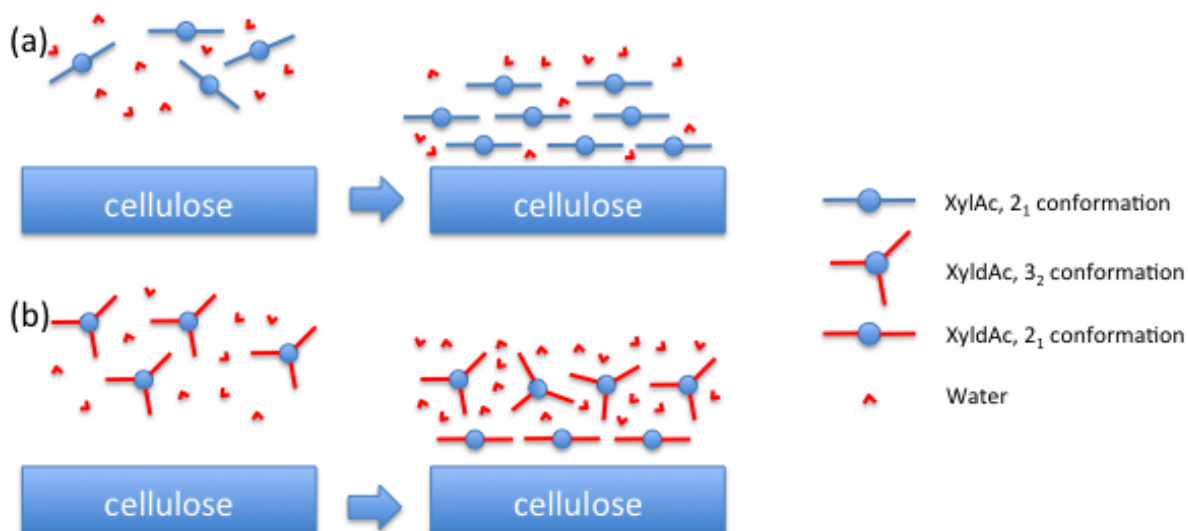
583 QCM-D experiments complemented by molecular modeling provide an atomistic-scale view  
584 of the effect of the acetyl groups attached to xylan on their adsorption on cellulose.

585 Adsorption of xylan fractions followed by QCM-D demonstrated that the acetylated and  
586 deacetylated fractions adsorption processes are both kinetically-driven but display different  
587 behaviors. XylAc has an almost homogenous adsorption pattern for all concentrations ( $k_f$

588 dominated), which suggests limited rearrangement after adsorption, whereas XyldAc displays  
589 two clear concentration domains of adsorption ( $k_1/k_2$  increased between 5 and 10 g L<sup>-1</sup>). These  
590 behaviors are also supported by the pattern of the  $\Delta D$  vs.  $\Delta f$  representation. The  $\Delta D$  vs.  $\Delta f$  plot  
591 for XylAc displays a single slope, whereas that for XyldAc shows two slopes between 2.5 and  
592 10 mg L<sup>-1</sup> of xylan injected. The slope change corresponds to the increase of the  $k_1/k_2$  ratio  
593 observed in the kinetic modeling analysis. For the higher slope (low concentration),  $k_1/k_2$  is  
594 close to one and increase when the slope become lower. The models revealed that adsorption  
595 of XylAc is straightforward since the acetylated xylan does not need to modify its solution  
596 conformation (two-fold helices). In contrast, adsorption of the very first molecules of XyldAc  
597 requires a conformational change to adopt a form complementary to that of cellulose (from  
598 three-fold to two-fold), whereas the additional molecules adsorb without conformation change  
599 (three-fold).

600 Additionally, the XylAc  $\Delta D$  vs.  $\Delta f$  slope displays a very low and homogeneous value ( $0.03 \cdot 10^6$   
601 Hz<sup>-1</sup>) compared to XyldAc fraction values that are higher and variable according to the  
602 concentration injected (from 0.5 to 0.1  $10^6$  Hz<sup>-1</sup>). This suggests the formation of a stiff and  
603 densely-packed XylAc layer, whereas the XyldAc fraction forms a more viscous layer that  
604 can be densified with increasing XyldAc concentration. In agreement with the experimental  
605 observations, the models also show that the acetyl groups affect the compactness and  
606 hydration of the xylan layer surrounding the cellulose. It is compact and weakly hydrated for  
607 acetylated xylan, but loose and highly hydrated for deacetylated xylan. Considering that water  
608 plasticizes hemicellulose, complexes made with XylAc would be rigid, as revealed by the low  
609 gradient of the  $\Delta D$  vs.  $\Delta f$  plot, whereas those made with XyldAc would be softer, showing a  
610 more viscous character, as suggested by the larger slopes of the  $\Delta D$  vs.  $\Delta f$  plot. The adsorption  
611 process of the acetylated and deacetylated xylylans on cellulose can be illustrated with the  
612 schematics shown in Fig. 6.

613



614

615 Fig. 6. Schematic representation of the adsorption process of XylAc (a) and XyldAc (b) on  
616 cellulose. Adsorption of XylAc results in the formation of a rigid (almost) anhydrous layer,  
617 whereas XyldAc forms a water-swollen soft layer.

618 Our findings indicated that the presence of acetyl esters influences the supramolecular  
619 organization of the xylan and its interaction with the cellulose surface. Deacetylated and  
620 acetylated xylans display different organization suggesting that the remaining substituent  
621 groups are not enough to keep the xylan interaction with cellulose surface unchanged. Indeed,  
622 in *Arabidopsis* mutants with decreased acetyl ester, compensation is provided by an increase  
623 in glucuronic (Grantham et al., 2017). In our case, the removal of all acetyl groups cannot be  
624 compensated by the other substituents.

625 The functional role of xylan in fleshy fruit remains unknown. In tomato, the trace amount of  
626 xylan was localized in cell walls lining intercellular space (Ordaz-Ortiz, Marcus, & Knox,  
627 2009) and particularly in the skin and inner epidermal cells of the pericarp (Takizawa et al.,  
628 2014). In biomass, it is found in the secondary wall (Carafa, Duckett, Knox, & Ligrone, 2005)  
629 and directly or indirectly contributes to the mechanical properties of the stems (Li et al., 2015;  
630 Dammstrom, Salmen, & Gatenholm, 2009). The biological and technological roles of acetyl

631 groups are still unclear but it has been hypothesized that they limit the saccharification and  
632 fermentation of biomass (Pawar et al., 2017). Besides the steric hindrance induced by acetyl  
633 groups to access a xylanase catalytic site, the formation of a poorly hydrated and stiff layer  
634 interacting with cellulose, as suggested by our study, can also be an explanation for the  
635 limited xylanase accessibility and mechanical properties of plant cell walls.

## 636 **CONCLUSION**

637 Combined QCM-D and MD approaches were used to illustrate the impact of acetyl decoration  
638 on the interaction between xylan and cellulose. Both *in vitro* and *in silico* results showed that  
639 acetyl groups attached to the xylan chains significantly influence the conformational behavior  
640 of xylan and the supramolecular organization of the cellulose-xylan complex. Acetylated  
641 fractions adsorbed on cellulose form a dense and poorly hydrated layer, whereas the  
642 deacetylated fraction forms a more hydrated layer. It should be noted that the acetylated  
643 fraction has the two residue per turn conformation for all the adsorbed chains, whereas this  
644 conformation is limited to the xylan chains in direct contact with the cellulose surface for the  
645 deacetylated fraction. Our study therefore supports the assumption that the acetylation pattern  
646 promotes different organizations and hydrations of xylan cellulose complexes that can  
647 modulate the interaction strength and rheological properties of the cell wall xylan-cellulose  
648 supramolecular complexes. Our future studies will focus on the evaluation of the influence of  
649 the presence of the acetyl groups on the properties as well as the use of the modulation of  
650 acetylation patterns to implement xylan/CNC-based composites.

651 **ASSOCIATED CONTENT**

652 **Supporting Information**

653 DOI:

654 **AUTHOR INFORMATION**

655 **Corresponding Author**

656 \*Email: Bernard.cathala@inra.fr

657 INRA, UR1268 Biopolymères Interactions Assemblages, Rue de la Géraudière, BP 71627,  
658 44316 Nantes, France.

659 Tel. 00 33 (0)2 40 67 50 68

660 **ACKNOWLEDGEMENTS**

661 We gratefully acknowledge the computational resources at the Centre d'Expérimentation et de  
662 Calcul Intensif, CECIC, ICMG, Grenoble. Part of this work was performed on the BIBS  
663 instrumental platform ([http://www.bibs.inra.fr/ bibs\\_eng/](http://www.bibs.inra.fr/bibs_eng/), UR1268 BIA, IBiSA, Phéno-  
664 Emphasis-FR ANR-11-INBS- 0012).

665



666 **REFERENCES**

- 667 Assor, C., Quemener, B., Vigouroux, J., & Lahaye, M. (2013). Fractionation and structural  
668 characterization of LiCl-DMSO soluble hemicelluloses from tomato. *Carbohydrate*  
669 *Polymers*, 94 (1), 46-55.
- 670 Bensefelt, T., Cranston, E. D., Ondaral, S., Johansson, E., Brumer, H., Rutland, M. W., &  
671 Wågberg, L. (2016). Adsorption of Xyloglucan onto Cellulose Surfaces of Different  
672 Morphologies: An Entropy-Driven Process. *Biomacromolecules*, 17(9), 2801-2811.
- 673 Berendsen, H. J. C., Postma, J. P. M., Van Gunsteren, W. F., & Hermans, J. (1981).  
674 Interaction models for water in relation to protein hydration. *Jerusalem Symp.*  
675 *Quantum Chem. Biochem.*, 14, 331-342.
- 676 Blumenkrantz, N., & Asboe-Hansen, G. (1973). New method for quantitative determination of  
677 uronic acids. *Analytical biochemistry*, 54, 484-489.
- 678 Bosmans, T. J., Stépán, A. M., Toriz, G., Renneckar, S., Karabulut, E., Wågberg, L., &  
679 Gatenholm, P. (2014). Assembly of Debranched Xylan from Solution and on  
680 Nanocellulosic Surfaces. *Biomacromolecules*, 15(3), 924-930.
- 681 Brummell, D. A., & Schröder, R. (2009). Xylan metabolism in primary cell walls. *New*  
682 *Zealand Journal of Forestry Science*, 30, 125-143.
- 683 Busse-Wicher, M., Gomes, T. C. F., Tryfona, T., Nikolovski, N., Stott, K., Grantham, N. J., . .  
684 . Dupree, P. (2014). The pattern of xylan acetylation suggests xylan may interact with  
685 cellulose microfibrils as a twofold helical screw in the secondary plant cell wall of  
686 *Arabidopsis thaliana*. *Plant Journal*, 79(3), 492-506.
- 687 Carafa, A., Duckett, J. G., Knox, J. P., & Ligrone, R. (2005). Distribution of cell-wall xylans  
688 in bryophytes and tracheophytes: new insights into basal interrelationships of land  
689 plants. *New Phytol*, 168(1), 231-240.

690 Chanzy, H., Dube, M., & Marchessault, R. H. (1979). Structural polymorphism of (1-4)-beta-  
691 D-xylan. *Polymer*, 20(8), 1037-1039.

692 Cherhal, F., Cousin, F., & Capron, I. (2015). Influence of Charge Density and Ionic Strength  
693 on the Aggregation Process of Cellulose Nanocrystals in Aqueous Suspension, as  
694 Revealed by Small-Angle Neutron Scattering. *Langmuir*, 31(20), 5596-5602.

695 Chong, S.-L., Virkki, L., Maaheimo, H., Juvonen, M., Derba-Maceluch, M., Koutaniemi, S., .  
696 . . Tenkanen, M. (2014). O-Acetylation of glucuronoxylan in *Arabidopsis thaliana*  
697 wild type and its change in xylan biosynthesis mutants. *Glycobiology*, 24(6), 494-506.

698 Dammak, A., Moreau, C., Beury, N., Schwikal, K., winter, H., Bonnin, E., . . . Cathala, B.  
699 (2013). Elaboration of multilayered thin films based on cellulose nanocrystals and  
700 cationic xylans: application to xylanase activity detection. *Holzforschung*, 67(5).

701 Dammstrom, S., Salmen, L., & Gatenholm, P. (2009). On the interactions between cellulose  
702 and xylan, a biomimetic simulation of the hardwood cell wall. *Bioresources*, 4(1), 3-  
703 14.

704 Darden, T., York, D., & Pedersen, L. (1993). Particle mesh Ewald: an N·log(N) method for  
705 Ewald sums in large systems. *J. Chem. Phys.*, 98, 10089-10092.

706 Dheilly, E., Le Gall, S., Guillou, M. C., Renou, J. P., Bonnin, E., Orsel, M., & Lahaye, M.  
707 (2016). Cell wall dynamics during apple development and storage involves  
708 hemicellulose modifications and related expressed genes. *Bmc Plant Biology*, 16.

709 Eronen, P., Osterberg, M., Heikkinen, S., Tenkanen, M., & Laine, J. (2011). Interactions of  
710 structurally different hemicelluloses with nanofibrillar cellulose. *Carbohydrate*  
711 *Polymers*, 86(3), 1281-1290.

712 Escudero, V., Jorda, L., Sopena-Torres, S., Melida, H., Miedes, E., Munoz-Barrios, A., . . .  
713 Molina, A. (2017). Alteration of cell wall xylan acetylation triggers defense responses

714 that counterbalance the immune deficiencies of plants impaired in the beta-subunit of  
715 the heterotrimeric G-protein. *Plant J*, 92(3), 386-399.

716 Evans, D. J., & Holian, B. L. (1985). The Nose-Hoover thermostat. *J. Chem. Phys.*, 83(8),  
717 4069-4074.

718 Falcoz-Vigne, L., Ogawa, Y., Molina-Boisseau, S., Nishiyama, Y., Meyer, V., Petit-Conil,  
719 M., Mazeau, K. Heux, L. (2017). Quantification of a tightly adsorbed monolayer of  
720 xylan on cellulose surface. *Cellulose (Dordrecht, Neth.)*, 24(9), 3725-3739.

721 Filisetti-Cozzi, T., & Carpita, N. (1991). Measurement of uronic acids without interference  
722 from neutral sugars. *Anal. Biochem.* 197(1), 1, 157-162.

723 Gabbay, S. M., Sundararajan, P. R., & Marchessault, R. H. (1972). X-ray and stereochemical  
724 studies on xylan diacetate. *Biopolymers*, 11(1), 79-94.

725 Gatenholm, P., & Tenkanen, M. (2004). *Hemicelluloses: Sciences and Technology*.  
726 Washington C, USA: American Chemical Society.

727 Grantham, N. J., Wurman-Rodrich, J., Terrett, O. M., Lyczakowski, J. J., Stott, K., Iuga, D., .  
728 . . Dupree, P. (2017). An even pattern of xylan substitution is critical for interaction  
729 with cellulose in plant cell walls. *Nature Plants*, 3(11), 859-865.

730 Kabel, M. A., van den Borne, H., Vincken, J.-P., Voragen, A. G. J., & Schols, H. A. (2007).  
731 Structural differences of xylans affect their interaction with cellulose. *Carbohydrate*  
732 *Polymers*, 69(1), 94-105.

733 Kittle, J. D., Qian, C., Edgar, E., Roman, M., & Esker, A. R. (2018). Adsorption of  
734 Xyloglucan onto Thin Films of Cellulose Nanocrystals and Amorphous Cellulose:  
735 Film Thickness Effects. *ACS Omega*, 3(10), 14004-14012.

736 Kohnke, T., Ostlund, A., & Brelid, H. (2011). Adsorption of Arabinoxylan on Cellulosic  
737 Surfaces: Influence of Degree of Substitution and Substitution Pattern on Adsorption  
738 Characteristics. *Biomacromolecules*, 12(7), 2633-2641.

739 Kubicki, J. D., Yang, H., Sawada, D., O'Neill, H., Oehme, D., & Cosgrove, D. (2018). The  
740 Shape of Native Plant Cellulose Microfibrils. *Scientific reports*, 8(1), 13983-13983.

741 Kumar, M., Campbell, L., & Turner, S. (2016). Secondary cell walls: biosynthesis and  
742 manipulation. *J Exp Bot*, 67(2), 515-531.

743 Larsson, P. T. (2004). *Interaction between cellulose I and hemicelluloses studied by spectral*  
744 *fitting of CP/MAS C-13-NMR spectra*. In P. Gatenholm & M. Tenhanen (Eds.),  
745 *Hemicelluloses: Science and Technology* (pp. 254-268)

746 Larsson, P. T., Hult, E. L., Wickholm, K., Pettersson, E., & Iversen, T. (1999). CP/MAS 13C-  
747 NMR spectroscopy applied to structure and interaction studies on cellulose I. *Solid*  
748 *State Nucl Magn Reson*, 15(1), 31-40.

749 Lee, S. H., Lee, H. L., & Youn, H. J. (2014). Adsorption and viscoelastic properties of  
750 cationic xylan on cellulose film using QCM-D. *Cellulose*, 21(3), 1251-1260.

751 Lee, S. H., Lee, H. L., & Youn, H. J. (2015). Adsorption of Xylan onto Cellulose Fibers  
752 Pretreated with Cationic Polyelectrolyte and Its Effect on Paper Properties.  
753 *Bioresources*, 10(1), 851-865.

754 Levigne, S., Thomas, M., Ralet, M. C., Quemener, B., & Thibault, J. F. (2002). Determination  
755 of the degrees of methylation and acetylation of pectins using a C18 column and  
756 internal standards. *Food Hydrocolloids*, 16(6), 547-550.

757 Li, L., Perre, P., Frank, X., & Mazeau, K. (2015). A coarse-grain force-field for xylan and its  
758 interaction with cellulose. *Carbohydr. Polym.*, 127, 438-450.

759 Linder, A., Bergman, R., Bodin, A., & Gatenholm, P. (2003). Mechanism of assembly of xylan  
760 onto cellulose surfaces. *Langmuir*, 19, 5072-5077.

761 Martinez-Abad, A., Berglund, J., Toriz, G., Gatenholm, P., Henriksson, G., Lindstrom, M., . .  
762 . Vilaplana, F. (2017). Regular Motifs in Xylan Modulate Molecular Flexibility and  
763 Interactions with Cellulose Surfaces. *Plant Physiology*, 175(4), 1579-1592.

764 Mazeau, K. (2011). On the external morphology of native cellulose microfibrils. *Carbohydr.*  
765 *Polym.*, 84(1), 524-532.

766 Mazeau, K., & Charlier, L. (2012). The molecular basis of the adsorption of xylans on  
767 cellulose surface. *Cellulose*, 19(2), 337-349.

768 Mazeau, K., & Charlier, L. (2012). The molecular basis of the adsorption of xylans on  
769 cellulose surface. *Cellulose (Dordrecht, Neth.)*, 19(2), 337-349.

770 Mazeau, K., Moine, C., Krausz, P., & Gloaguen, V. (2005). Conformational analysis of xylan  
771 chains. *Carbohydrate Research*, 340(18), 2752-2760.

772 Mazeau, K., Moine, C., Krausz, P., & Gloaguen, V. (2005). Conformational analysis of xylan  
773 chains. *Carbohydrate research*, 340(18), 2752-2760.

774 Melton, L. D., Smith, B. G., Ibrahim, R., & Schröder, R. (2009). Mannans in primary and  
775 secondary plant cell walls. *New Zealand J. Forestry Sci.*, 39, 153-160.

776 Mortimer, J. C., Faria-Blanc, N., Yu, X., Tryfona, T., Sorieul, M., Ng, Y. Z., . . . Dupree, P.  
777 (2015). An unusual xylan in Arabidopsis primary cell walls is synthesised by GUX3,  
778 IRX9L, IRX10L and IRX14. *The Plant Journal*, n/a-n/a.

779 Nieduszynski, I., & Marchessault, R. H. (1971). Structure of  $\beta$ -D-(1-4) xylan hydrate. *Nature*  
780 *(London)*, 232(5305), 46-47.

781 Nieduszynski, I. A., & Marchessault, R. H. (1972). Structure of  $\beta$ ,D(1-4')-xylan hydrate.  
782 *Biopolymers*, 11(7), 1335-1344.

783 Nishiyama, Y., Langan, P., & Chanzy, H. (2002). Crystal structure and hydrogen-bonding  
784 system in cellulose I $\beta$  from synchrotron X-ray and neutron fiber diffraction. *J. Am.*  
785 *Chem. Soc.*, 124(31), 9074-9082.

786 Ordaz-Ortiz, J. J., Marcus, S. E., & Knox, J. P. (2009). Cell wall microstructure analysis  
787 implicates hemicellulose polysaccharides in cell adhesion in tomato fruit pericarp  
788 parenchyma. *Molecular Plant*, 2, 910-921.

789 Pawar, P. M., Derba-Maceluch, M., Chong, S. L., Gomez, L. D., Miedes, E., Banasiak, A., . .  
790 . Mellerowicz, E. J. (2016). Expression of fungal acetyl xylan esterase in *Arabidopsis*  
791 *thaliana* improves saccharification of stem lignocellulose. *Plant Biotechnol J*, 14(1),  
792 387-397.

793 Pawar, P. M.-A., Derba-Maceluch, M., Chong, S.-L., Gandla, M. L., Bashar, S. S., Sparrman,  
794 T., . . . Mellerowicz, E. J. (2017). In muro deacetylation of xylan affects lignin  
795 properties and improves saccharification of aspen wood. *Biotechnology for Biofuels*,  
796 10.

797 Quemener, B., Vigouroux, J., Rathahao, E., Tabet, J. C., Dimitrijevic, A., & Lahaye, M.  
798 (2015). Negative electrospray ionization mass spectrometry: a method for sequencing  
799 and determining linkage position in oligosaccharides from branched hemicelluloses.  
800 *Journal of Mass Spectrometry*, 50, 247-264.

801 Ralet, M. C., Williams, M. A. K., Tanhatan-Nasseri, A., Ropartz, D., Quemener, B., &  
802 Bonnin, E. (2012). Innovative Enzymatic Approach to Resolve Homogalacturonans  
803 Based on their Methylesterification Pattern. *Biomacromolecules*, 13(5), 1615-1624.

804 Rappe, A. K., Casewit, C. J., Colwell, K. S., Goddard, W. A., III, & Skiff, W. M. (1992).  
805 UFF, a full periodic table force field for molecular mechanics and molecular dynamics  
806 simulations. *J. Am. Chem. Soc.*, 114(25), 10024-10035.

807 Rappe, A. K., & Goddard, W. A., III. (1991). Charge equilibration for molecular dynamics  
808 simulations. *J. Phys. Chem.*, 95(8), 3358-3363.

809 Ray, S., Vigouroux, J., Quemener, B., Bonnin, E., & Lahaye, M. (2014). Novel and diverse  
810 fine structures in LiCl-DMSO extracted apple hemicelluloses. *Carbohydrate*  
811 *Polymers*, 108, 46-57.

812 Revol, J. F., Bradford, H., Giasson, J., Marchessault, R. H., & Gray, D. G. (1992). Helicoidal  
813 self-ordering of cellulose microfibrils in aqueous suspension. *International Journal of*  
814 *Biological Macromolecules*, 14(3), 170-172.

815 Rojas, O. J. (2016). *Cellulose Chemistry and Properties: Fibers, Nanocelluloses and*  
816 *Advanced Materials*: Springer.

817 Sauerbrey, G. (1959). *Z. Phys.*, 155, 206.

818 Scheller, H. V., & Ulvskov, P. (2010). Hemicelluloses. *Annual Review of Plant Biology*,  
819 61(1), 263-289.

820 Sims, I. M., Craik, D. J., & Bacic, A. (1997). Structural characterisation of  
821 galactoglucomannan secreted by suspension-cultured cells of *Nicotiana*  
822 *plumbaginifolia*. *Carbohydrate Research*, 303, 79-92.

823 Takizawa, A., Hyodo, H., Wada, K., Ishii, T., Satoh, S., & Iwai, H. (2014). Regulatory  
824 specialization of xyloglucan (XG) and glucuronoarabinoxylan (GAX) in pericarp cell  
825 walls during fruit ripening in tomato (*Solanum lycopersicum*). *Plos One*, 9, e89871.

826 Teleman, A., Larsson, P. T., & Iversen, T. (2001). On the accessibility and structure of xylan  
827 in birch kraft pulp. *Cellulose*, 8(3), 209-215.

828 Thibault, J. F. (1979). Automatisation du dosage des substances pectiques par laméthode au  
829 meta-hydroxydiphenyl. *Lebensmittel-Wissenschaft & Technologie*, 12, 247-251.

830 Tollier, M. T., & Robin, J. P. (1979). Adaption de la méthode à l'orcinol-sulfurique au  
831 dosage automatique des glucides neutres totaux: Conditions d'application aux extraits  
832 d'origine végétale. *Annals des Technologies agricoles*, 28, 1-15.

833 Verlet, L. (1967). Computer "experiments" on classical fluids. I. Thermodynamical properties  
834 of Lennard-Jones molecules. *Phys. Rev.*, 159(1), 98-103.

- 835 Villares, A., Bizot, H., Moreau, C., Rolland-Sabate, A., & Cathala, B. (2017). Effect of  
836 xyloglucan molar mass on its assembly onto the cellulose surface and its enzymatic  
837 susceptibility. *Carbohydrate Polymers*, 157, 1105-1112.
- 838 Villares, A., Moreau, C., Capron, I., & Cathala, B. (2014). Chitin Nanocrystal-Xyloglucan  
839 Multilayer Thin Films. *Biomacromolecules*, 15(1), 188-194.
- 840 Villares, A., Moreau, C., Dammak, A., Capron, I., & Cathala, B. (2015). Kinetic aspects of  
841 the adsorption of xyloglucan onto cellulose nanocrystals. *Soft Matter*, 11(32), 6472-  
842 6481.
- 843 Voragen, F., Schols, H., & Visser, R. (2003). Advances in pectin and pectinase research.  
844 *Annals of Botany*, 94, 479-480.
- 845 York, W. S., Oates, J. E., van Halbeek, H., Darvill, A., & Albersheim, P. (1988). Location of  
846 the *O*-acetyl substituents on a nonasaccharide repeating unit of sycamore extracellular  
847 xyloglucan. *Carbohydrate Research*, 173, 113-132.
- 848 Yuan, Y., Teng, Q., Zhong, R., & Ye, Z. H. (2016). Roles of Arabidopsis TBL34 and TBL35  
849 in xylan acetylation and plant growth. *Plant Sci*, 243, 120-130.

850